ANNALS OF GEOPHYSICS, 69, 5, GP555, 2026; doi:10.4401/ag-9592
OPEN ACCESS

Aeromagnetic data interpretation for structural architecture modeling in the Boke region, Northwestern Guinea

Adama Sangaré[1], Lahsen Achkouch[*,1,2], Younesse El Cheikh[1], Mohammad Taadid[1], Mohammed Boumehdi[2], Younes Mamouch[1], Daouda Diakité[3], Ahmed Rachid[1], Ahmed Attou[1]

(1) Hassan First University of Settat, Faculty of Sciences and Technology, Laboratory Physico Chemistry of Processes and Materials, Research Team Geology of the Mining and Energetics Resources, Settat 26002, Morocco
(2) National Office of Hydrocarbons and Mines, 5, Moulay Hassan Street, Rabat 10020, Morocco
(3) Ministry of Mines and Geology, Republic of Guinea

Article history: received April 25, 2026; accepted August 13, 2026

Abstract

The Boke region, in north-western Guinea, lies at the Atlantic margin of the West African Craton, where an Archean to Paleoproterozoic basement is largely concealed beneath the Paleozoic sedimentary cover of the Bowe Basin and a thick lateritic mantle. This setting hosts the Fouta Djallon-Mandingo bauxite province, yet its concealed structure remains poorly documented. To characterize this structure aeromagnetic data were interpreted using an integrated workflow combining reduction to the equator, upward continuation, the analytic signal, the horizontal gradient amplitude, the tilt derivative, the tilt angle of the horizontal gradient (TAHG), and Euler deconvolution. The interpretation resolves three magnetic domains, two positive anomalies (PMA1 and PMA2), attributed to concealed mafic bodies deep Birimian or Archean mafic basement and shallow Mesozoic dolerite intrusions, respectively separated by a broad negative anomaly (NMA1) that corresponds to the weakly magnetic sedimentary fill of the Bowe Basin. Euler deconvolution yields source depths from about 400 m to 9,600 m, the deepest sources forming an arcuate band in the north and the shallowest contacts dissecting the central basin. The magnetic lineaments, classified by length into three orders, define a polyphase fault network in which the most frequent set trends WNW-ESE to E-W and reflects an inherited basement fabric, whereas the tectonically most significant set corresponds to the NE-SW to ENE-WSW transform system, with subordinate NW-SE and N-S structures. The multi-level analysis reveals a depth-stratified architecture in which a dense, shallow, brittle fabric passes downward into a few deep, curvilinear structures indicative of ductile shear, interpreted as an inherited Eburnean-Pan-African transcurrent framework overprinted by Mesozoic, rift-related brittle faulting. Beyond refining the tectonic architecture of this segment of the craton margin, the delineated fault and fracture framework particularly the structural intersections provides a structural guide to the fault-controlled development of the region's lateritic bauxite.

Keywords: Aeromagnetic data; Structural mapping; Magnetic lineaments; Upward continuation; TAHG; Euler deconvolution; West African Craton; Boke; Republic of Guinea

1. Introduction

The Boke region occupies the north-western part of the Republic of Guinea, on the Atlantic margin of the West African Craton (Fig. 1). It lies at the western edge of the Leono-Liberien massif, where an Archean to Paleoproterozoic crystalline basement, consolidated during the Liberian and Eburnean (~2.2-2.0 Ga) orogenic cycles (Bessoles, 1977; Boher et al., 1992; Grenholm et al., 2019), is largely concealed beneath the Paleozoic sedimentary cover of the Bowe Basin (Mamedov et al., 2010a). This basement was subsequently reworked during the Pan-African orogeny and, above all during the Mesozoic break-up of Gondwana and the opening of the Atlantic Ocean, which reactivated major fault systems and emplaced large dolerite and gabbro-dolerite intrusions across western Guinea (Mamedov et al., 2010a). This succession of tectonic and magmatic events, combined with intense Cenozoic lateritic weathering, gave rise to the Fouta Djallon-Mandingo province, one of the largest bauxite districts in the world (Mamedov et al., 2010a; Barry et al., 2021), making the region a prime target for both structural and mineral-exploration studies.

Aeromagnetic surveying is one of the most effective geophysical methods for regional geological and structural mapping, particularly in areas where dense vegetation, lateritic weathering, or sedimentary cover obscures the bedrock (Cordell and Grauch, 1985; Nabighian et al., 2005; Bouiflane et al., 2017; Ouchchen et al., 2021; Ibraheem et al., 2019). By exploiting contrasts in the magnetic properties of rocks, it enables the delineation of lithological boundaries, faults, and other subsurface discontinuities, while imaging buried magnetic bodies, such as dolerite intrusions concealed beneath sedimentary cover (Blakely et al., 1995; Nabighian et al., 2005; Hinze et al., 2013; Mamouch et al., 2023; Ouchchen et al., 2021). Consequently, the interpretation of aeromagnetic data provides a solid basis for reconstructing the structural framework of a region and constitutes an essential tool for mineral exploration by identifying structures and lithological features that may control mineralization (Grant, 1972; Miftah et al., 2017; Ouchchen et al., 2021; Mohamed et al., 2022).

A wide range of processing techniques has been developed to enhance and map magnetic lineaments. Reduction to the equator repositions anomalies over their sources in low-latitude regions (Baranov and Naudy, 1964), and upward continuation separates the responses of shallow and deep sources (Henderson and Zietz, 1949; Jacobsen, 1987; Mamouch et al., 2023). Derivative-based filters like the horizontal gradient amplitude (Blakely and Simpson, 1986), the analytic signal, which locates sources independently of magnetization direction (Nabighian, 1972; Roest et al., 1992), the tilt derivative (Miller and Singh, 1994; Salem et al., 2008) and the tilt angle of the horizontal gradient (TAHG), which sharpens edge detection and resolves curvilinear structures (Ferreira et al., 2013), are the most widely used tools for detecting and enhancing the magnetic signatures of tectonic structures. Euler deconvolution complements these edge detectors by estimating the depth and position of the causative sources (Thompson, 1982; Reid et al., 1990). Applied together, and especially when computed at several continuation levels, these methods allow a structural network to be mapped and its geometry to be tracked as a function of depth.

Despite its economic importance, the Boke region has received relatively limited attention from the perspective of regional structural interpretation. Government airborne geophysical surveys conducted in 1980-1981 and the extensive exploration campaigns of the 1970s established the region as one of the world's major bauxite provinces (Wright et al., 1985; Mamedov et al., 2010a). Building on these datasets, the present study applies an integrated interpretation of aeromagnetic data using reduction to the equator, upward continuation at four levels, the analytic signal, horizontal gradient amplitude, tilt derivative, multi-level TAHG with automated extraction of local maxima, and Euler deconvolution. The objectives are threefold: (i) to interpret the magnetic anomalies and delineate the concealed fault and lineament network; (ii) to characterize the magnetic domains and estimate the depth of their sources in order to reconstruct the depth-dependent structural architecture of the basement; and (iii) to relate this structural framework to the regional tectonic evolution and to the structural controls governing the development of the lateritic bauxite cover.

2. Geological setting

2.1 Regional context

The study area belongs to the West African Craton, one of the Precambrian shields that, together with the Congo, Kalahari and Tanzania cratons, form the ancient nucleus of the African continent (Bessoles, 1977; Boher et al., 1992). The craton consists of an Archean to Paleoproterozoic crystalline basement, extensively migmatised, granitised and

metamorphosed, which is unconformably overlain along its margins by Neoproterozoic to Palaeozoic sedimentary cover (Boulangé et al., 1996; Mamedov et al., 2010a; Barry et al., 2021). In Guinea, this basement corresponds to the Leono-Liberien massif, a domain of Archean migmatites, granite-greenstone belts and granulite-facies series exposed in the centre and south-east of the country, which passes north-westward, beneath the Atlantic coastal margin, into Palaeozoic sequences capped by Cenozoic deposits (Mamedov et al., 2010a; Sidibe and Yalcin, 2019). The north-western region of Guinea, which constitutes the study area, lies within this cover domain and is underlain by a Palaeozoic clastic succession comprising the Ordovician Pita Formation (quartzitic sandstones, gravels and conglomerates passing up into mudstones and siltstones), the Silurian Telimele Formation (argillites, siltstones and shales) and the Devonian Faro Formation (fine-grained sandstones, siltstones and mudstones), as shown on the geological map (Fig. 1) (Mamedov et al., 2010a; Barry et al., 2021; Sangaré et al., 2024).

2.2 Local context

The Boke region occupies the western, peripheral part of the Bowe syncline, on the south-western flank of the Taoudeni syneclise, and forms part of the Fouta Djallon-Mandingo bauxite province developed along the western margin of the West African Craton (Mamedov et al., 2010b; Mamedov et al., 2021). The area is characterized by a thick, gently dipping sedimentary succession ranging from the Ordovician to the Devonian, including the Pita, Telimele and Faro formations described above which is intruded locally by Mesozoic mafic trap rocks and capped by widespread lateritic weathering profiles. The region hosts some of the world's largest bauxite deposits, which are developed mainly on the weathered Devonian and post-Devonian shales, mudstones, siltstones, and sandstones, with a smaller contribution from weathered Mesozoic dolerite and gabbro-dolerite intrusions (Hoppe, 1977; Mamedov et al., 2010a; Barry et al., 2021; Sangaré et al., 2024).

Although the Boke area is largely covered by the Paleozoic sedimentary succession and its lateritic mantle, its present-day structural framework reflects the long and polyphase evolution of the underlying West African Craton. The crystalline basement preserves the imprint of the successive Liberian (Archean), Eburnean (Palaeoproterozoic, 2.2-2.0 Ga), and Pan-African tectonic events, which collectively controlled the cratonization, deformation, and reworking of the basement (Bessoles, 1977; Boher et al., 1992; Mamedov et al., 2010a). During the Mesozoic, this Precambrian framework was further modified by the break-up of Gondwana and the opening of the Atlantic Ocean, which reactivated major basement fault systems across western Guinea and promoted the emplacement of dolerite intrusions along these inherited structures (Mamedov et al., 2010a; Mamedov et al., 2021; Makarova et al., 2019; Akaemov, 1975).

The structural framework of the study area is dominated by NE-SW to ENE-WSW faults, accompanied by subordinate NW-SE and E-W fracture systems (Mamedov et al., 2010a). The NE-trending faults belong to the regional transform system associated with the opening of the Atlantic Ocean and are particularly developed in the Cap Verga coastal region, which includes the study area. The NW-SE and E-W fracture sets represent conjugate structures that were repeatedly reactivated and served as pathways for the emplacement of mafic intrusions (Mamedov et al., 2010a). Together, these inherited structures controlled the regional geomorphology, drainage pattern, distribution of mafic trap rocks, and the development of lateritic weathering and bauxite deposits, resulting in the structural compartmentalization of the region. Because much of this fault network is concealed beneath the sedimentary cover and lateritic mantle, its geometry cannot be fully resolved from surface geology alone. Aeromagnetic data therefore provide an effective means of imaging and characterizing these buried structural features.

3. Data and methods

The aeromagnetic data used in this study were acquired between 1980 and 1981 by Amtec Resources Management Ltd on behalf of the Guinean Ministry of Mines and Geology. The survey was flown along NE-SW traverse lines spaced 1 km apart, with NW-SE tie lines every 10 km, at a mean terrain clearance of 120 m, and the total magnetic field was sampled every 50 m along the flight lines. The recorded total magnetic intensity was reduced following standard potential-field protocols (Reeves, 2005; Nabighian et al., 2005; Telford et al., 1990). Time-varying external contributions were removed through a diurnal correction (Nabighian et al., 2005; Telford et al., 1990), and residual line-to-line levelling errors were suppressed by micro-levelling with a 2 nT tolerance (Minty, 1991). The core-field contribution

was then removed by subtracting the International Geomagnetic Reference Field (IGRF) appropriate to the survey epoch, isolating the crustal anomaly field. The resulting Residual Magnetic Field (RMF) was interpolated onto a regular grid (cell size ≈ one-quarter of the line spacing) using the minimum-curvature algorithm, which yields the smoothest surface consistent with the observations while limiting the spurious oscillations that can arise near steep gradients and geological boundaries (Briggs, 1974; Swain, 1976; Smith and Wessel, 1990).

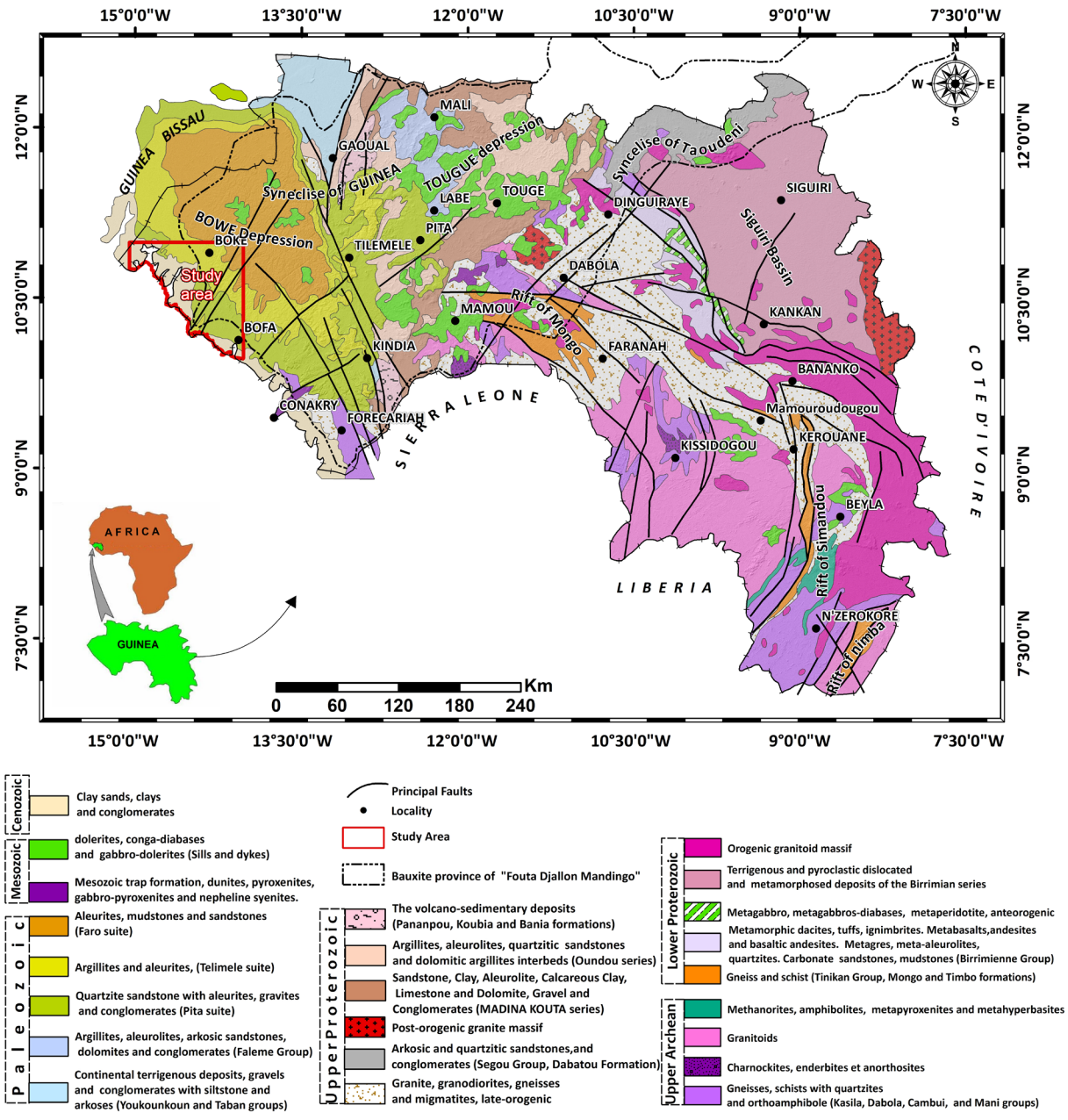


Figure 1. Geological Map of Guinea Showing Major Lithological Units and Structural Features with the Location of the Study Area (Mamedov et al., 2010b; Sangaré et al., 2024).

3.1 Field transformations and edge detection

The methodological approach combines qualitative and quantitative techniques, with the qualitative phase specifically contributing to improving data readability and geological interpretability. In low magnetic latitude regions (inclination < 15°) such as the study area, reduction to the pole (RTP) is numerically unstable. The low inclination amplifies noise and produces strong N-S elongation of anomalies along the declination azimuth (Blakely et al., 1995;

Jayeoba and Odumade, 2015; Shehu et al., 2017). Reduction to the Equator (RTE) was therefore preferred to relocate anomalies symmetrically over their causative bodies while avoiding the directional distortion inherent to RTP at low latitudes (Awoyemi et al., 2018; Hartman et al., 1971). The transform was applied in the wavenumber domain using the field inclination and declination computed for the survey epoch from the IGRF. The resulting magnetic grids were subsequently used to compute five complementary enhancement transforms, including (i) upward continuation (UC), (ii) the analytic signal (AS), (iii) the horizontal gradient amplitude (HGA), (iv) and the tilt derivative (TDR) for qualitative edge detection, followed by the total amplitude of the horizontal gradient (TAHG) and Euler deconvolution (ED) for source depth estimation and structural mapping following the workflow in Fig. 2.

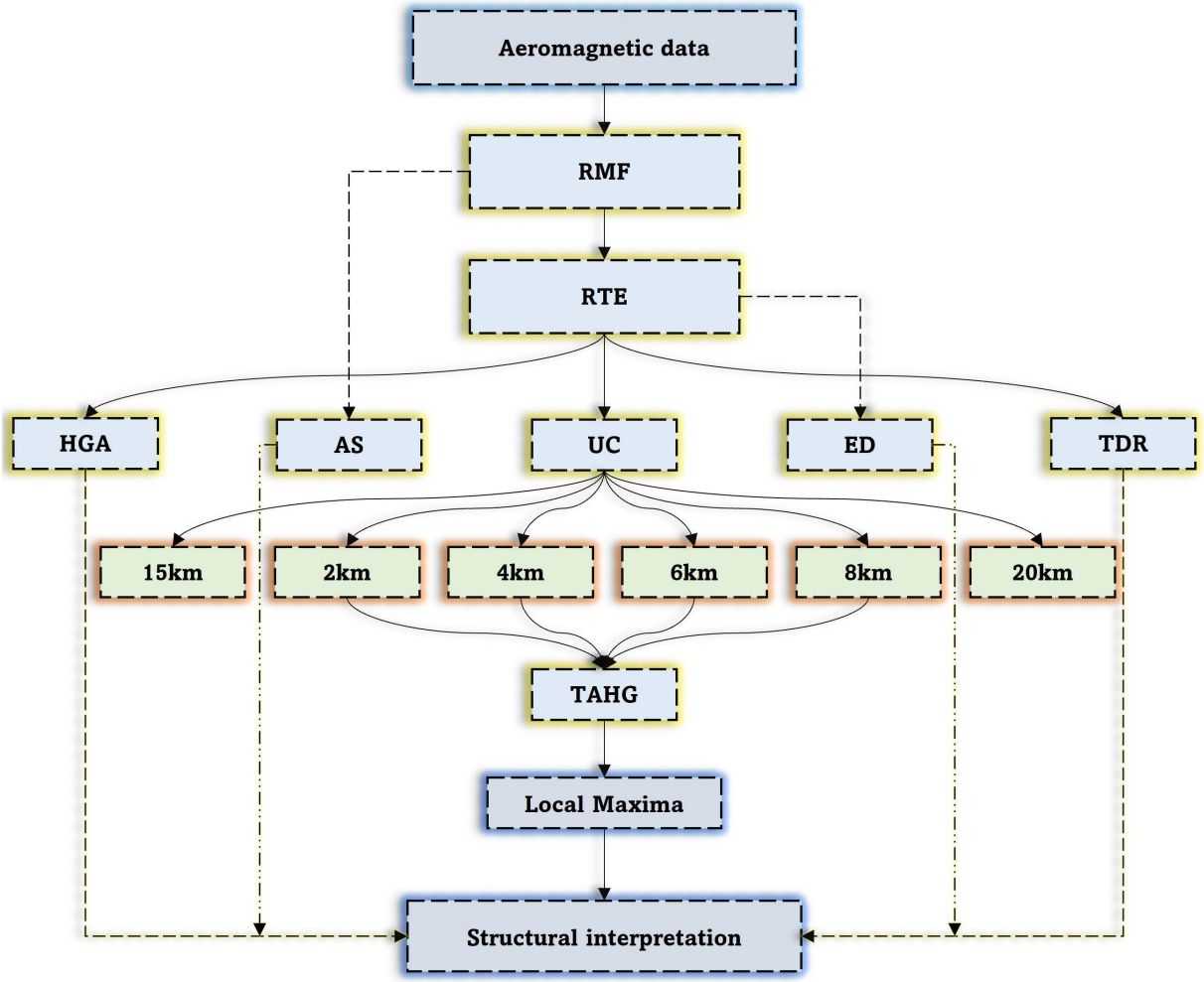


Figure 2. Processing workflow of the magnetic data illustrating the methodology adopted to accomplish the study objectives.

Upward continuation recomputes the field as if it had been measured on a higher horizontal plane and behaves as a low-pass filter that attenuates short-wavelength, near-surface signals while preserving the long-wavelength response of deeper sources (Henderson and Zietz, 1949; Jacobsen, 1987; Blakely et al., 1995; Mamouch et al., 2023). In the wavenumber domain it is a multiplication by:

$$U(k) = e^{-h|k|} \tag{1}$$

where $|k|$ is the radial wavenumber and h the continuation height. The field was continued to six levels, including four closely spaced heights ($h = 2$, 4, 6, and 8 km) and two higher levels ($h = 15$ and 20 km). These closely and regularly spaced levels were chosen to build a finely sampled, depth-stratified set of grids that allows structural lineaments to be tracked continuously from shallow to mid-crustal levels, rather than relying on a few widely spaced

heights, as h increases, shallow signals fade and deep-seated sources progressively dominate (Jacobsen, 1987; Zhu et al., 2022; Mamouch et al., 2023). The four closely spaced levels (2-8 km) provided the grids used for the multi-level TAHG edge analysis, whereas the two higher levels (15 and 20 km) were computed specifically to provide an independent, regional-scale discrimination of the relative depths of the magnetic domains (Fig. 4e-f). The multiscale edge analysis derived from these continued grids (TAHG and local maxima) is developed below under source depth estimation and structural mapping.

The amplitude of the analytic signal was derived from the three orthogonal gradients of the residual magnetic field (Nabighian, 1972; Roest et al., 1992):

$$AS(x,y) = \sqrt{\left(\frac{\partial M}{\partial x}\right)^2 + \left(\frac{\partial M}{\partial y}\right)^2 + \left(\frac{\partial M}{\partial z}\right)^2} \tag{2}$$

where *M* is the RMF field. By combining the vertical and horizontal derivatives, the *AS* amplitude is largely independent of the magnetization direction and the ambient field orientation, and its maxima occur approximately over the edges and corners of the sources. This makes it particularly valuable at the low inclination of the study area, where amplitude-dependent filters are most affected (Roest et al., 1992). It was therefore used as an independent constraint on source location alongside the HGA, TDR, and ED solutions.

The HGA measures the maximum lateral rate of change of the field and produces ridges (local maxima) that overlie the lateral edges of magnetic sources such as faults, contacts, and dyke margins (Cordell and Grauch, 1985; Blakely and Simpson, 1986). It is defined as:

$$HGA(x,y) = \sqrt{\left(\frac{\partial M}{\partial x}\right)^2 + \left(\frac{\partial M}{\partial y}\right)^2} \tag{3}$$

The HGA is effective for delineating both shallow and deep magnetic sources, but its maxima can be displaced from the true edge when contacts dip steeply or when sources are closely spaced (Grauch and Cordell, 1987; Phillips, 2007; Benyas et al., 2021). To mitigate the amplitude dependence of the HGA, the tilt derivative of Miller and Singh (1994) was computed by normalizing the vertical derivative by the horizontal-gradient amplitude:

$$TDR(x,y) = \tan^{-1}\left(\frac{\frac{\partial M}{\partial z}}{\sqrt{\left(\frac{\partial M}{\partial x}\right)^2 + \left(\frac{\partial M}{\partial y}\right)^2}}\right) \tag{4}$$

The TDR is bounded between −90° and +90° irrespective of anomaly amplitude, which equalizes the response of weak and strong sources and makes it effective in noisy or multi-source settings (Verduzco et al., 2004; Salem et al., 2008; Marson and Klingele, 1993). Among its useful properties, the zero contour of the TDR closely tracks the lateral edges of magnetic bodies, while the horizontal separation between its +45° and −45° contours over a near-vertical contact can provide a first-order estimate of source depth (Salem et al., 2007; Verduzco et al., 2004; Mamouch et al., 2023). In this study, the TDR was used to trace and map structural lineaments and contacts, taking advantage of its stability where amplitude-dependent filters lose resolution over weakly magnetized sources.

3.2 Source depth estimation and structural mapping

For quantitative interpretation, standard Euler deconvolution (Thompson, 1982; Reid et al., 1990) was applied to the RTE grid to estimate the horizontal position and depth of magnetic sources. The method solves Euler's homogeneity equation:

$$(x - x_0)\frac{\partial M}{\partial x} + (y - y_0)\frac{\partial M}{\partial y} + (z - z_0)\frac{\partial M}{\partial z} = N(B - M) \tag{5}$$

where (x_0, y_0, z_0) are the coordinates of the source, B is the regional (background) field, and N is the structural index (SI), a parameter that describes the geometry of the assumed source and controls the estimated depth. The SI is diagnostic of source type, ranging from contacts and faults ($N \approx 0$) through dykes, sills, and steps ($N \approx 0.5$-1) to cylinders and compact bodies ($N \approx 2$-3). Since the aim of this study was to map magnetic lineaments, a structural index of $N = 0$ was adopted, corresponding to contact- and fault-type sources. A 10×10-cell moving window and a 15% depth tolerance were applied to reject poorly constrained solutions and limit the scatter of the depth estimates (Reid et al., 2014).

To delineate magnetic lineaments, the tilt angle of the total horizontal gradient (TAHG) of Ferreira et al. (2013) was applied to each upward-continued grid. The TAHG normalizes the horizontal-gradient amplitude defined in Eq. (3) by taking its tilt angle:

$$TAHG\ (x,y) = \tan^{-1}\left(\frac{\frac{\partial HGA}{\partial z}}{\sqrt{\left(\frac{\partial HGA}{\partial x}\right)^2 + \left(\frac{\partial HGA}{\partial y}\right)^2}}\right) \tag{6}$$

where HGA is the horizontal gradient amplitude of the upward-continued field. As a normalized derivative, the TAHG balances the responses of shallow and deep sources, generating well-defined maxima over source boundaries while effectively suppressing spurious edge responses (Ferreira et al., 2013). Its ridge crests were extracted as local maxima marking the horizontal position of magnetic contacts at each continuation height. Superimposing the local-maxima sets obtained at 2, 4, 6, and 8 km then yields a multiscale edge map in which shallow-source edges appear only at low continuation heights and fade as h increases, whereas deep-rooted structures persist across successive levels, allowing lineaments to be traced continuously from shallow to mid-crustal depths.

4. Results

4.1 Field transformations and edge detection

4.1.1 Residual magnetic field and reduction to the equator

The residual magnetic field (RMF) map (Fig. 3a) and its reduction-to-the-equator (RTE) transformation (Fig. 3b) provide the foundation for the structural interpretation. The RMF exhibits magnetic values ranging from approximately −227 nT to 217 nT, with strong positive anomalies concentrated in the northern and southern parts of the study area, while a marked negative anomaly characterizes the central and central-eastern sectors. The observed anomalies show a predominantly N-S orientation and a lateral displacement typical of low-latitude magnetic fields, where anomaly peaks are shifted from their causative sources. The RTE transformation corrects this displacement by centering the anomalies over their sources, thereby improving the spatial correlation between magnetic signatures and geological structures. This enhancement provides a more reliable framework for the subsequent structural mapping and depth-estimation analyses.

The RTE map (Fig. 3b) reveals magnetic intensities ranging from approximately −200 nT to 209 nT, indicating significant contrasts in magnetic susceptibility between the geological units. Three major magnetic domains can be distinguished: (i) a large positive magnetic anomaly (PMA1) in the northern and north-western part of the study area, (ii) a dominant negative magnetic anomaly (NMA1) occupying the central sector and extending eastward, and (iii) a second positive magnetic anomaly (PMA2) of high amplitude located in the south-eastern region near Bofa. The town of Boke is situated along the irregular boundary separating PMA1 from NMA1. The close spatial association of strong positive and negative anomalies suggests a structurally complex basement composed of blocks with contrasting magnetic properties. These three magnetic domains provide the main structural framework for the interpretation of the subsequent magnetic enhancement and depth-analysis results.

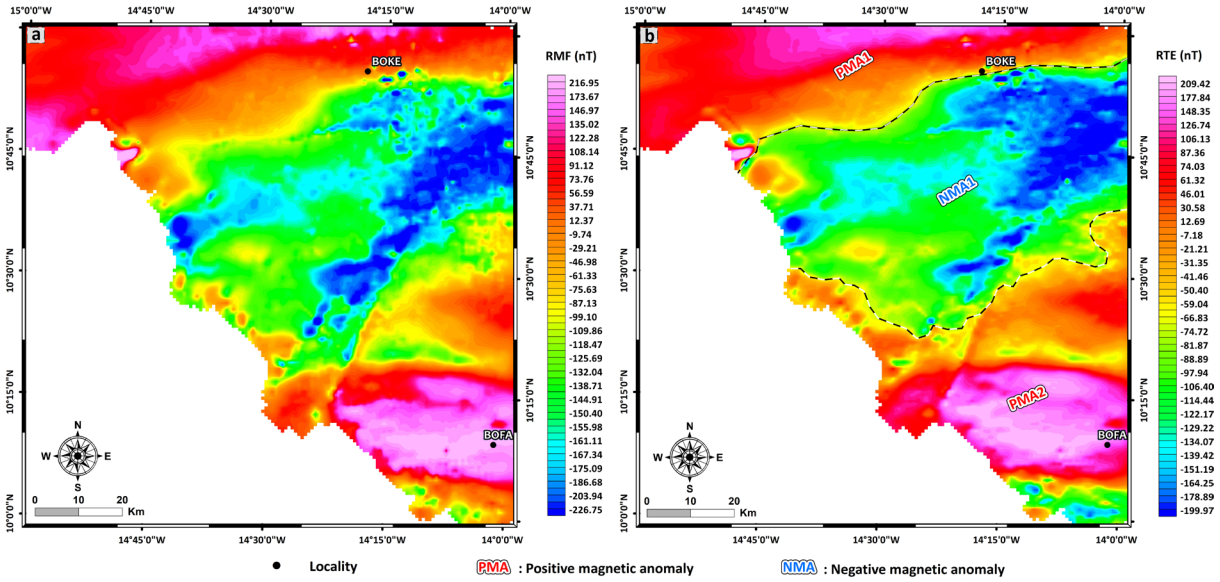


Figure 3. Residual magnetic field of the study area (a) and its reduction-to-the-equator (RTE) transform (b).

4.1.2 Upward Continuation

Upward continuation was applied to the RTE field at heights of 2, 4, 6, and 8 km, and at two higher levels of 15 and 20 km (Fig. 4a-f) to progressively suppress shallow magnetic effects and enhance the regional response associated with deeper sources. Despite the increasing continuation height, the three main magnetic domains (PMA1, NMA1, and PMA2) remain clearly identifiable. The numerous short-wavelength anomalies visible at 2 km, particularly within NMA1 and along the margins of PMA1, gradually disappear with increasing altitude, producing a smoother magnetic field dominated by broad regional anomalies at 8 km. PMA1 in the north and NMA1 in the central part of the study

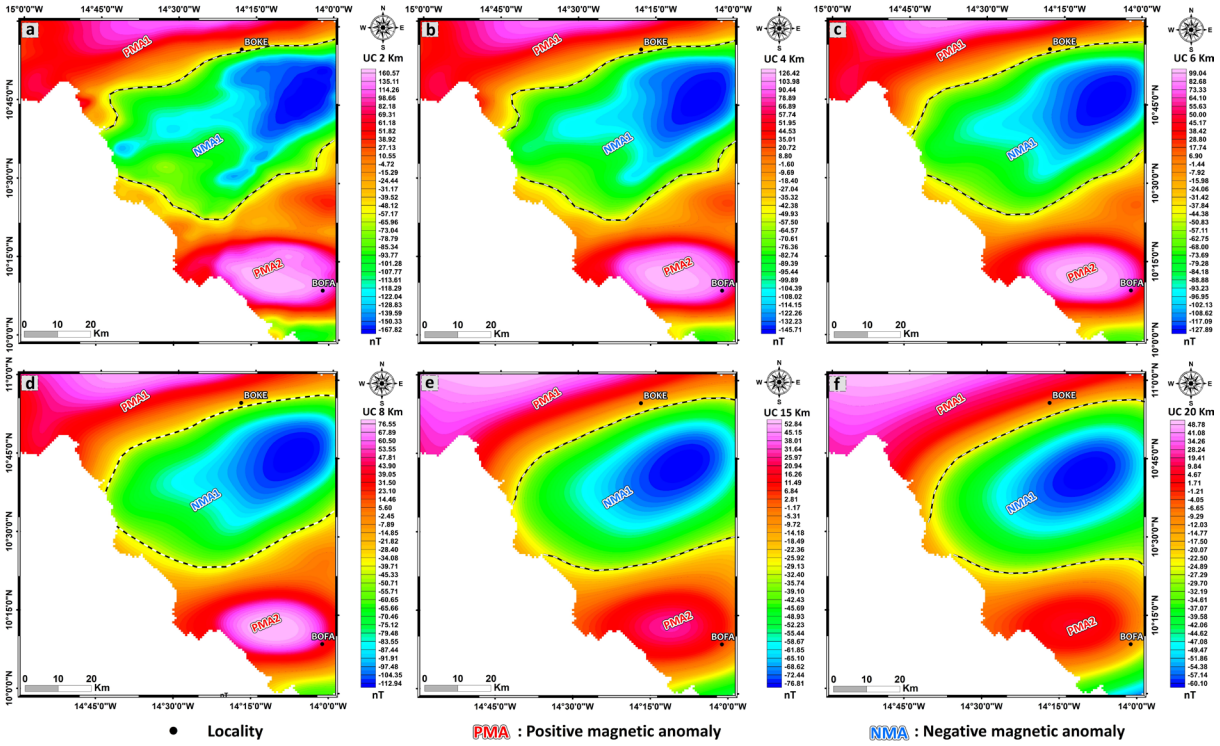


Figure 4. Upward continuation of the RTE field to 2 km (a), 4 km (b), 6 km (c) and 8 km (d), 15 km (e) and 20 km (f).

area remain the most prominent features throughout the continuation sequence, indicating the presence of deep and laterally extensive magnetic sources. PMA2 in the south-eastern sector also persists at all levels, although its amplitude decreases more noticeably and its spatial extent becomes slightly reduced, suggesting a comparatively shallower source. This contrast becomes explicit at the higher continuation levels 15 and 20 km (Fig. 4e-f), where PMA1 remain strongly expressed, whereas PMA2 attenuates markedly and its amplitude decreases faster than that of PMA1, providing an independent, domain-scale confirmation that PMA2 is shallower than the deeply rooted PMA1 domain. The preservation of the three magnetic domains up to 8 km confirms that the first-order magnetic framework is controlled by deep-seated geological structures, whereas the attenuated short-wavelength anomalies reflect shallower structural features. The relative depths of these magnetic sources are further constrained by the Euler deconvolution results (Section 4.2.3).

4.1.3 Analytic Signal

The analytic signal amplitude (Fig. 5), which ranges from 0.001 to 1.111 nT/m, was computed to locate the edges and tops of magnetic sources independently of the direction of magnetization a property of particular value in the low-latitude setting of the study area, where reduction-based products remain sensitive to residual inclination effects. The AS map is dominated by a prominent, sinuous high-amplitude belt that traverses the central part of the area in a broadly NNE-SSW direction, together with pervasive high AS across the southern and south-eastern

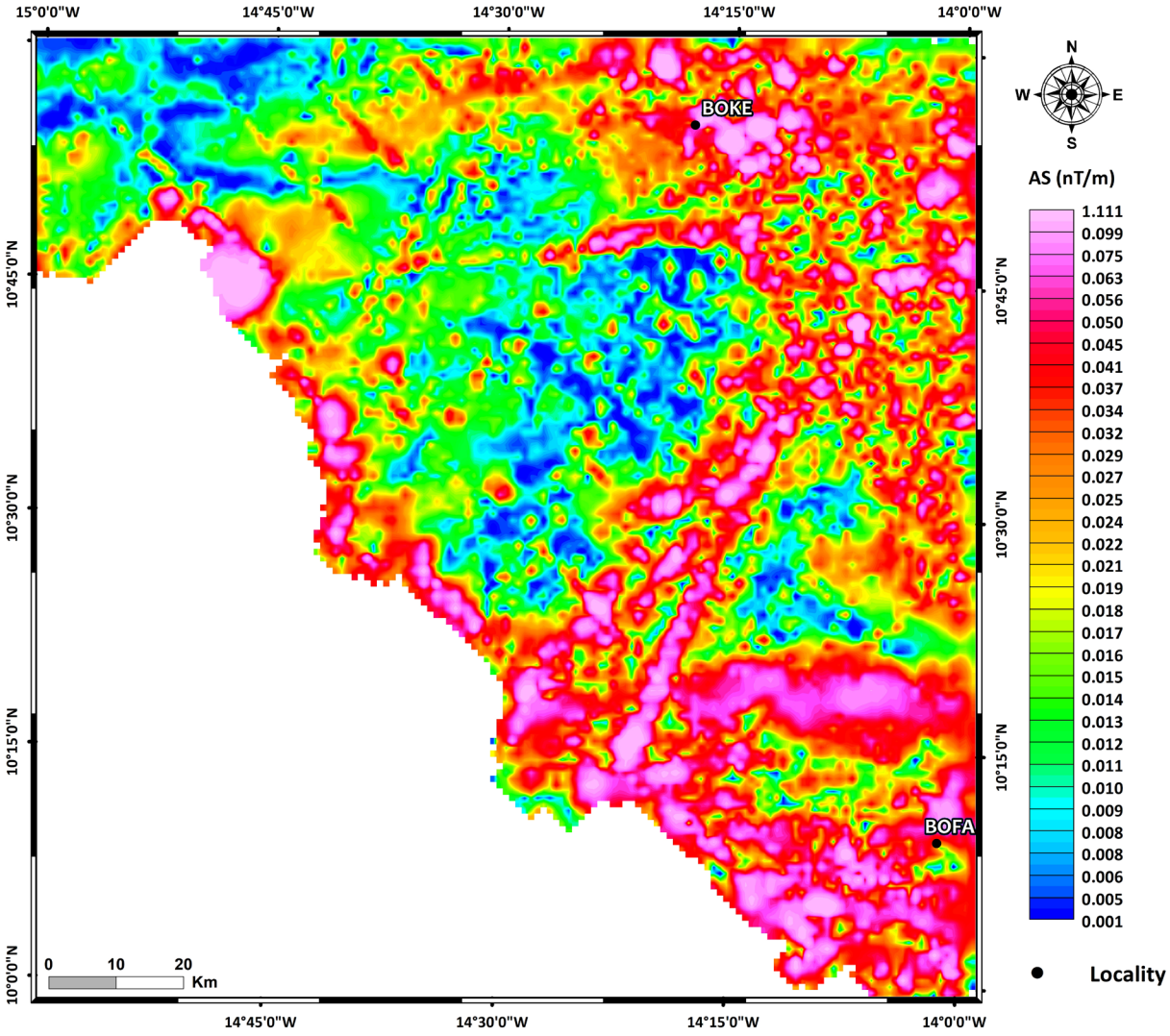


Figure 5. Analytic signal amplitude of the magnetic field of the study area.

sectors, including the PMA2 domain and the southern margin. These sharp, high-amplitude maxima delineate shallow, strongly magnetized sources and steep, near-vertical contacts. Localized high-AS responses also mark the northern PMA1 boundary in the vicinity of Boke.

In contrast, low AS amplitudes dominate the north-western sector and the core of the central NMA1 domain, reflecting smoother magnetic gradients could be associated with deeper or less strongly magnetized sources. The marked contrast between the high-amplitude southern anomalies and the low-amplitude response of NMA1 supports a difference in source depth and geometry, with the southern structures and the central magnetic belt corresponding to relatively shallow, well-defined sources, while the NMA1 core is linked to deeper or more diffuse magnetic bodies. Because the analytic signal is independent of magnetization direction, these features confirm that the identified magnetic domains and their boundaries represent real geological structures rather than artefacts related to low-latitude magnetic effects.

4.1.4 Horizontal gradient amplitude and Tilt derivative

The horizontal gradient amplitude (HGA) map (Fig. 6a), with values ranging from 0.001 to 0.083 nT/m, was used to identify zones of strong lateral magnetic contrast, where high values indicate sharp geological contacts and faults. The most prominent feature is a narrow, continuous high-gradient lineament extending through the central part of the study area in a NNE-SSW direction, suggesting a major fault or near-vertical structural boundary. High-gradient zones are also observed in the southern and south-eastern sectors, where they form elongated E-W to ENE-WSW trends along the margins of the PMA2 domain. Additional high-gradient anomalies delineate the northern boundary of PMA1 near Boke. In contrast, the central part of the NMA1 domain is characterized by low gradient values, reflecting a relatively homogeneous magnetic response away from major contacts.

The tilt derivative (TDR) map (Fig. 6b), with values ranging from −1.48 to 1.48 rad, enhances magnetic sources regardless of their amplitude, allowing both shallow and deep structures to be detected with similar clarity. Compared with the HGA map, the TDR reveals a denser and more continuous network of structural lineaments across the study area, including the central-eastern sector where the HGA response is relatively weak. This demonstrates the ability of the TDR to highlight subtle and deeply rooted structures that may not be clearly resolved by amplitude-based filters. The structural fabric is dominated by NE-SW to ENE-WSW trends, locally changing to E-W in the southern sector. These trends are intersected by a major NNE-SSW lineament in the central part of the area. The coincidence of HGA and TDR anomalies along the boundaries between PMA1 and NMA1, as well as between NMA1 and PMA2, indicates that these contacts may represent major crustal-scale discontinuities.

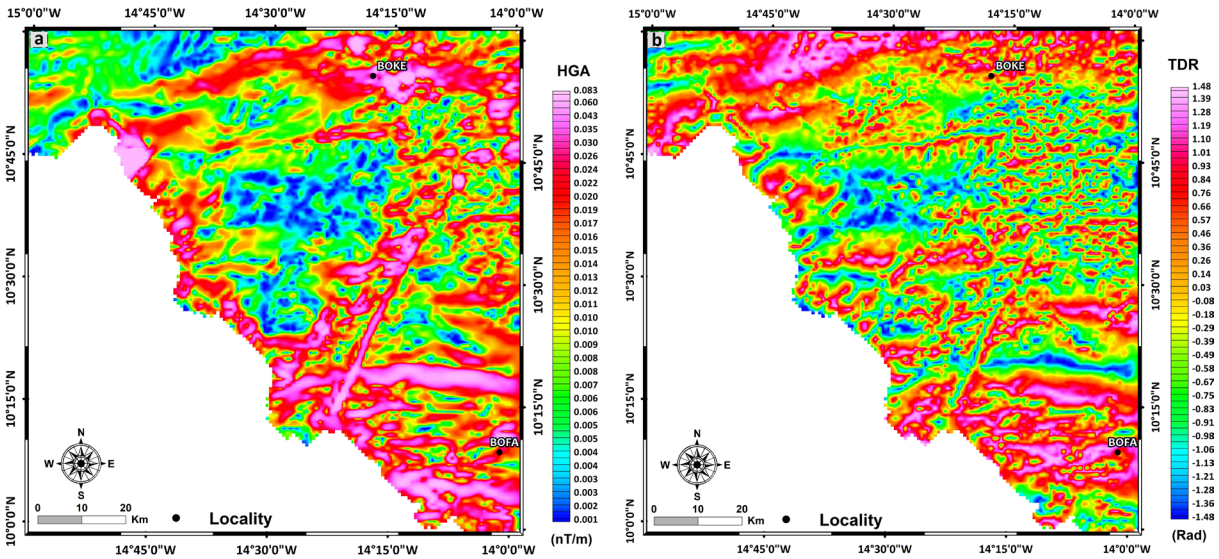


Figure 6. Horizontal gradient amplitude (a) and tilt derivative (b) of the RTE field.

4.2 Source depth estimation and structural mapping

4.2.1 Multi-level tilt angle of the horizontal gradient

The tilt angle of the horizontal gradient (TAHG) was computed on each of the four upward-continued grids (2, 4, 6 and 8 km; Fig. 7a-d) in order to map the structural fabric as a function of depth. Because the TAHG normalizes the horizontal-gradient response and balances the expression of shallow and deep edges, applying it across a series of continuation levels images how the structural network evolves with increasing source depth.

At the 2 km level (Fig. 7a), the TAHG map reveals a dense network of short and closely spaced lineaments with multiple orientations, although NE-SW to ENE-WSW and E-W trends are predominant. This pattern reflects the complexity of the shallow structural fabric. As the continuation height increases to 4 and 6 km (Fig. 7b, c), many of the short-wavelength features disappear, while the remaining structures become longer, more continuous, and easier to trace. At these depths, several broad curvilinear and sigmoidal lineaments become clearly visible. At the 8 km level (Fig. 7d), only the most persistent regional structures remain. These include a major ENE-WSW to E-W lineament system in the northern part of the study area, characterized by distinct sigmoidal bends, as well as broad curved structures in the southern sector. The progressive simplification of the structural pattern with increasing depth represents a key result of this study. The shallow levels are dominated by numerous short and rectilinear

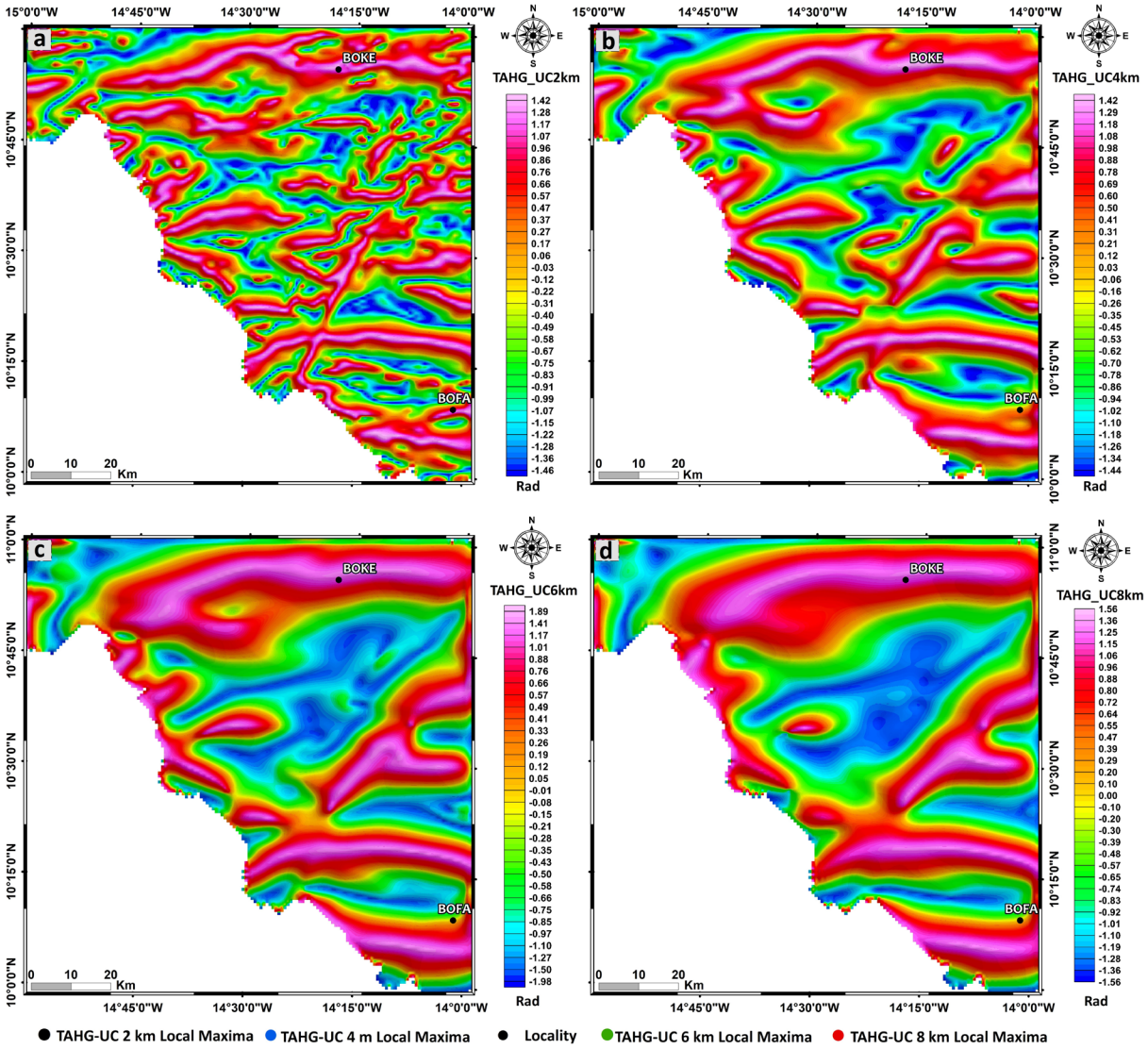


Figure 7. Tilt angle of the horizontal gradient (TAHG) computed on the upward-continued fields at 2 km (a), 4 km (b), 6 km (c) and 8 km (d).

lineaments, whereas the deeper levels are characterized by fewer but longer and more continuous curvilinear structures. While part of this smoothing is an inherent effect of upward continuation, which acts as a low-pass filter, the deeper structures do not merely become fewer but retain a distinct curvilinear and sigmoidal geometry, indicating a genuine structural organization rather than a purely filtering response. The persistence of these curved and sigmoidal features at depth suggests that they are deep-seated geological structures, likely related to major shear zones. This contrast indicates a vertical variation in deformation style, with brittle structures predominating near the surface and more ductile deformation affecting the deeper crust.

4.2.2 TAHG Local Maxima

The local maxima of the TAHG were extracted from the four upward-continuation levels (2, 4, 6, and 8 km) and combined allowing shallow and deep structural features to be visualized simultaneously (Fig. 8). This approach provides an objective and reproducible representation of the structural framework by highlighting the crest lines of magnetic edges.

The resulting lineament map reveals a dense structural network dominated by ENE-WSW to E-W trends, accompanied by NE-SW and NW-SE lineaments, with a few N-S structures. The colour distribution clearly illustrates the depth organization of the structural system. Deep-level maxima (red, 8 km) form long, smooth, and continuous lineaments that represent the major crustal-scale structures, including the arcuate to sigmoidal feature identified in the northern part of the study area (inset a). In contrast, shallow-level maxima (black, 2 km) are more numerous, shorter, and less continuous, reflecting the complexity of the near-surface structural fabric. The highest concentration of lineaments occurs in the central sector and along the boundaries between the main magnetic domains, indicating zones of intense deformation. The enlarged views highlight key structural features, including a central intersection

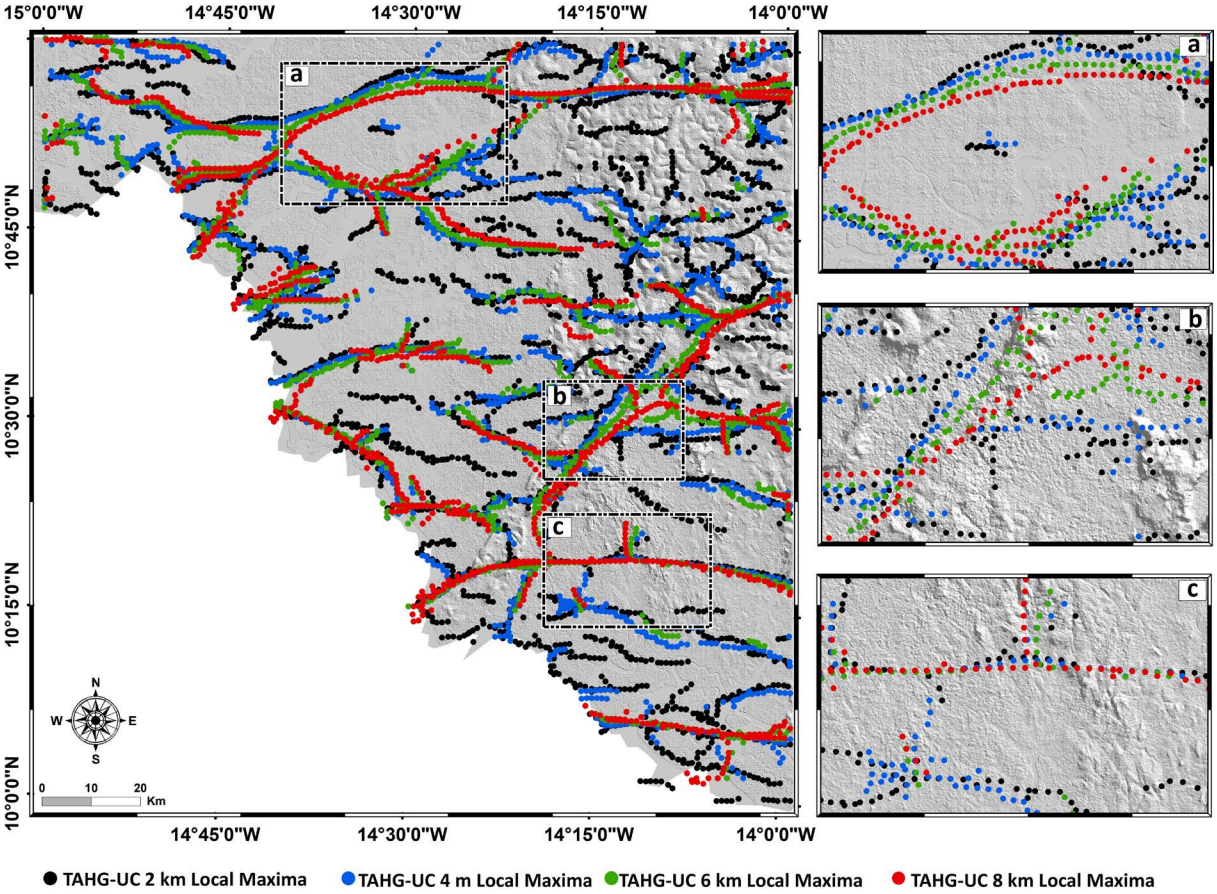


Figure 8. Local maxima map of the TAHG derived from four upward-continuation levels (black: 2 km; blue: 4 km; green: 6 km; red: 8 km).

zone where E-W, NE-SW, and NW-SE lineaments converge (inset b), and a major E-W structure crosscut by shorter N-S lineaments in the south-central sector (inset c).

The spatial relationship between TAHG maxima at successive continuation levels also provides qualitative information on the dip of geological structures. Where maxima from all four levels are closely superimposed, the corresponding structure is interpreted as steeply dipping or vertical. In contrast, a progressive lateral displacement of maxima with increasing continuation height indicates an inclined structure, with the direction of displacement corresponding to the dip direction. This relationship can be observed in the enlarged areas of Fig. 8. In inset a, the maxima associated with different continuation levels are systematically displaced along the arcuate northern structure, suggesting inclined surfaces. In inset b, variable offsets between maxima indicate the presence of structures with different dip orientations. In inset c, the maxima of the major E-W lineament are largely superimposed, indicating a steep to near-vertical structure. The coexistence of vertical and inclined lineaments supports the interpretation of a complex and multi-stage deformation history affecting the study area.

4.2.3 Euler Deconvolution

Euler deconvolution was applied to estimate the depth and location of the magnetic sources (Fig. 9). To provide an interpretation consistent with the resolving capability of the method, the solutions are presented as four broad depth classes (≈400-2000 m, 2000-3800 m, 3800-6000 m, and 6000-9600 m), highlighting the main depth trends rather than individual solution depths. The estimated solutions extend from approximately 400 m to 9,600 m across the study area and define three principal depth populations that correspond closely to the three magnetic domains identified on the RTE map. The deepest solutions (6000-9600 m class) are associated with the northern PMA1 domain

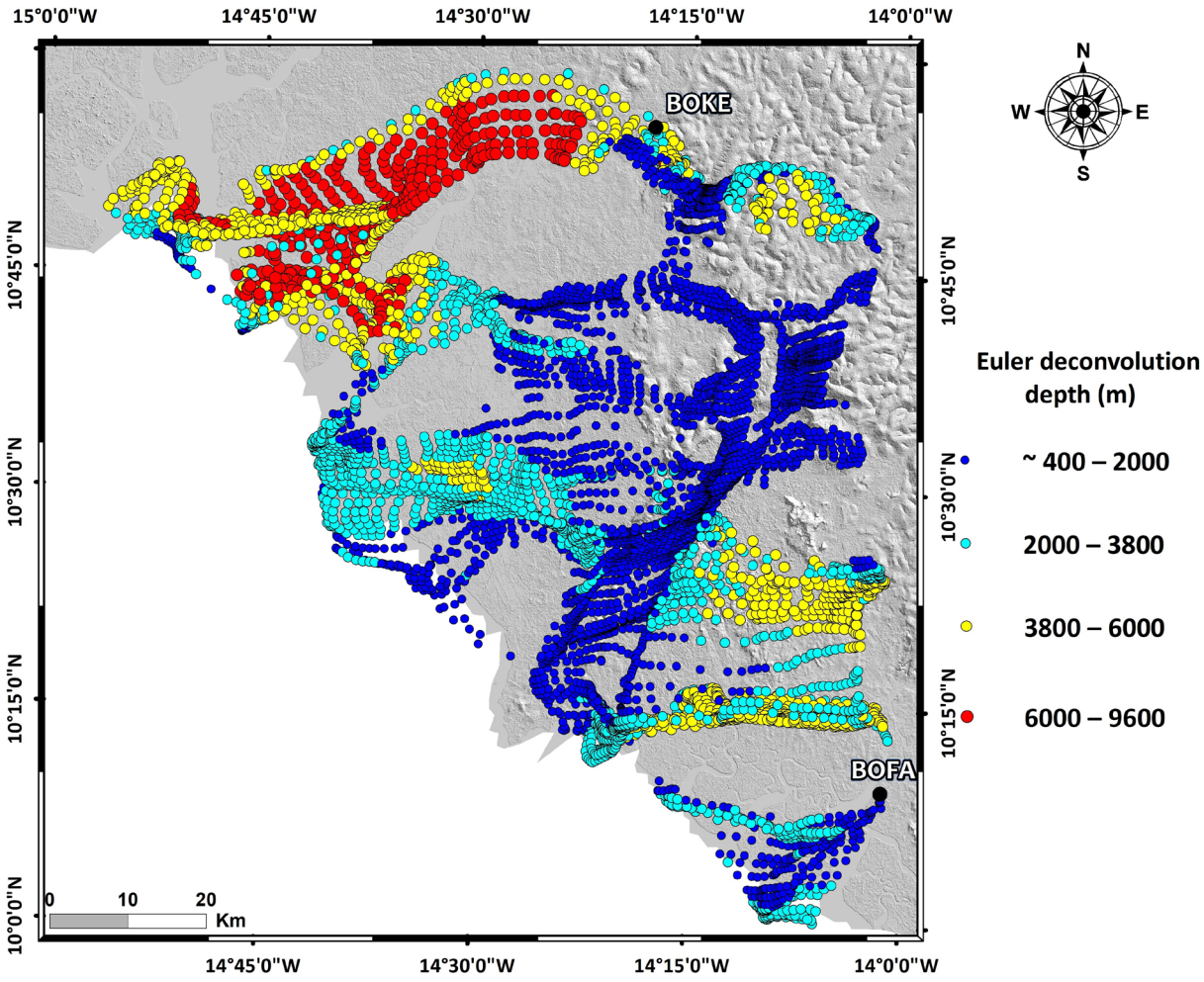


Figure 9. Euler deconvolution solutions showing the estimated depths of the magnetic sources.

and define an arcuate to locally sigmoidal band that follows the northern boundary of the domain. These deep sources are interpreted as deeply rooted basement bodies, most plausibly mafic intrusions or high-susceptibility crustal blocks concealed beneath the sedimentary cover. The PMA2 domain, in the south-eastern sector, is characterized by intermediate depths, largely falling within the 2000-6000 m classes.

In contrast, the central NMA1 domain is dominated by the shallowest solutions (≈400-2000 m class, locally up to the lower part of the 2000-3800 m class). These shallow sources are arranged along NE-SW to ENE-WSW trends, outlining a network of structural discontinuities. Although NMA1 remains clearly expressed on the upward-continuation maps, the Euler results show that the structures controlling its internal geometry are relatively shallow. NMA1 therefore corresponds to a broad regional magnetic low dissected by numerous shallow faults and contacts. The overall depth relationship among the three domains is thus PMA1 (deepest) > PMA2 (intermediate) > NMA1 (shallowest).

Considering the inherent uncertainty of Euler deconvolution, the estimated values should be regarded as depth ranges rather than exact depths. The solutions are not randomly distributed but are aligned along ENE-WSW to NE-SW trends, with a subordinate NW-SE orientation, consistent with the structural framework revealed by the magnetic edge-detection filters. Furthermore, the arcuate to sigmoidal geometry of the deepest PMA1 solutions closely matches the deep curvilinear structures identified on the multi-level TAHG maps. This agreement between two independent approaches supports the interpretation of a deep-seated shear zone in the northern part of the study area. The close spatial relationship between the deepest magnetic sources and the major structural lineaments suggests that both were controlled by the same tectonic processes.

5. Discussion

The aeromagnetic interpretation can be understood within the regional geological framework of north-western Guinea. The study area is located at the north-western margin of the West African Craton, within the Leono-Liberien (Kenema-Man) massif, where the Archean to Paleoproterozoic crystalline basement is largely buried beneath the Upper Proterozoic to Paleozoic sedimentary cover of the Bowe Basin, situated on the south-western flank of the Taoudeni Syneclise (Mamedov et al., 2010b). The basement has experienced a long and complex geological evolution, including Archean cratonization, Paleoproterozoic Eburnean (~2.2-2.0 Ga) tectono-metamorphic consolidation within the Birimian framework of the West African Craton (Grenholm et al., 2019), Pan-African (Late Riphean-Cambrian) reactivation along the Rokel-Bassari mobile belt, and Mesozoic reactivation associated with the breakup of Gondwana and the opening of the Atlantic Ocean (Mamedov et al., 2010a).

Within this geological framework, the three magnetic domains identified on the RTE map can be assigned clear geological significance. The central negative magnetic anomaly (NMA1), characterized by a broad, long-wavelength magnetic low and relatively shallow bounding contacts (~400-2000 m), corresponds to the Bowe Basin. The geological map (Fig. 1) shows that this area is mainly covered by weakly magnetic sedimentary rocks, including the argillites and aleurites of the Telimele formation, the quartzitic sandstones of the Pita formation, the sandstones of the Faro formation, and Cenozoic clays along the north-western coastal plain. The low magnetic susceptibility of these sedimentary units explains the observed magnetic low. The persistence of NMA1 after upward continuation indicates the large lateral extent of the sedimentary basin, whereas the shallow Euler solutions delineate the faults that bound and compartmentalize the basin, some of which coincide with the major faults shown on the geological map.

Given that the sedimentary cover is essentially non-magnetic, the positive magnetic anomalies (PMA1 and PMA2) are unlikely to originate from surface lithologies and are instead interpreted as the expression of strongly magnetized mafic bodies concealed beneath the sedimentary sequence. This geological setting highlights the value of aeromagnetic data, which are capable of imaging subsurface magnetic sources that lack surface exposure. This interpretation is consistent with the regional survey, which identified buried mafic intrusive bodies as positive magnetic anomalies beneath the Pita-suite cover (Mamedov et al., 2010a). In addition, the geological map (Fig. 1) indicates that the regional mafic magmatism comprises Mesozoic dolerites, conga-diabases, and gabbro-dolerites emplaced as sills and dykes, together with older anteorogenic Birimian metagabbros. The relatively high magnetic susceptibility of these mafic lithologies compared with the surrounding sedimentary rocks (Clark, 1999; Mamedov et al., 2010a) provides a consistent explanation for the observed positive magnetic response. The contrasting depths of the two positive magnetic anomalies indicate two distinct expressions of the regional mafic magmatic

record. The relatively shallow sources associated with PMA2 (2000-6000 m) are consistent with Mesozoic dolerite sills and dykes emplaced within the sedimentary cover, a style of magmatism very widely developed in the neighbouring Telimele-Kindia-Koumbia region as part of the Mesozoic trap event (Mamedov et al., 2010a). The shallow character of PMA2 is independently supported by the upward-continuation results, as PMA2 attenuates markedly at the higher continuation levels (15 and 20 km), whereas the deep PMA1 domain persists, confirming the depth contrast between the two positive anomalies. In contrast, the deeper PMA1 sources (6000-9,600 m), which form an arcuate-to-sigmoidal trend, are more plausibly interpreted as concealed mafic basement bodies, most likely Birimian metagabbros or Archean mafic units, emplaced or preserved along a major deep-seated structural zone. This interpretation is supported by the regional geological framework, the mapped lithostratigraphy, and the characteristic magnetic properties of mafic rocks.

The magnetic lineaments extracted from the horizontal gradient, tilt derivative, and multi-level TAHG were integrated to produce a synthetic structural map of the study area. Based on their length, the mapped lineaments were classified into three hierarchical orders: (i) first-order lineaments (>20 km), representing 12% of the total population, (ii) second-order lineaments (5-20 km), accounting for 40%, (iii) and third-order lineaments (<5 km), constituting 48% (Fig. 10a, c). This hierarchical distribution characterized by a limited number of regional-scale structures and a predominance of short fractures, is typical of well-developed fault systems that have undergone multiple episodes of deformation. The rose diagram (Fig. 10b) identifies four principal structural trends: NE-SW to ENE-WSW, WNW-ESE to E-W, NW-SE, and N-S to NNE-SSW. These orientation families are consistent with the regional tectonic framework and reflect successive phases of crustal deformation documented in the geological evolution of the area (Mamedov et al., 2010a).

The NE-SW to ENE-WSW trend corresponds to the regional Mesozoic transform fault system associated with the breakup of Gondwana and the opening of the Atlantic Ocean. These transform structures are concentrated within the Cap Verga coastal domain, which includes the study area, and exerted a major control on the emplacement of Mesozoic mafic magmatism, including dolerite, gabbro-dolerite, and associated ultramafic intrusions (Mamedov et al., 2010a). Their orientation also coincides with the NE-ENE structural grain that characterizes the Birimian terranes of the West African Craton (Grenholm et al., 2019), suggesting that the Mesozoic transform system preferentially reactivated inherited Eburnean basement fabrics. The N-S to NNE-SSW family, represented by a prominent first-order sinuous lineament crossing the central part of the study area, is interpreted as a deeply rooted basement discontinuity. Regionally, this structural direction corresponds to the submeridian fault zones that controlled the development of the Bassari-Rokel trough system and partitioned the Precambrian basement into large crustal blocks (Mamedov et al., 2010a). These structures therefore represent an inherited basement framework, probably established during the Pan-African or earlier tectonic events and subsequently reactivated during later magmatic episodes. The NW-SE lineaments coincide with the regional fault systems that delimit the terrigenous graben-syncline structures and locally guided the emplacement of dolerite dyke swarms (Mamedov et al., 2010a). Their spatial distribution suggests that this orientation acted primarily as an extensional structural direction accommodating basin development and magmatic intrusion. The WNW-ESE to E-W trend represents another significant structural family. Regional geological studies identify this orientation as a distinct tectonic direction inherited from an earlier, possibly early Paleozoic deformational phase (Mamedov et al., 2010a). It is therefore interpreted as an inherited basement fabric that was locally reactivated during subsequent tectonic events. Furthermore, several NE-trending faults in the southeastern part of the country progressively curve into E-W orientations (Fig. 1), producing sigmoidal geometries indicative of transcurrent deformation within ductile shear zones. These four lineament families record a polyphase tectonic evolution, in which inherited submeridian and sublatitudinal basement structures were successively reactivated and overprinted by NE-oriented transcurrent faulting associated with Mesozoic Atlantic rifting. This structural framework is consistent with the principal fault network depicted on the geological map (Fig. 1).

The integrated interpretation of the multi-level TAHG and Euler deconvolution results reveals a systematic variation in structural style with depth. At shallow continuation levels, the magnetic fabric is characterized by a dense network of short, rectilinear, and multidirectional lineaments, typical of brittle upper-crustal deformation. In contrast, increasing continuation height progressively suppresses these shallow features, revealing a simplified structural framework dominated by a limited number of long, curvilinear, and locally sigmoidal lineaments, particularly within the arcuate northern domain. This depth-dependent evolution is consistent with the hierarchical organization of the synthetic structural map (Fig. 10), where the first-order lineaments (>20 km; 12% of the mapped population) correspond to regional structures that remain identifiable at continuation levels of 6-8 km, whereas

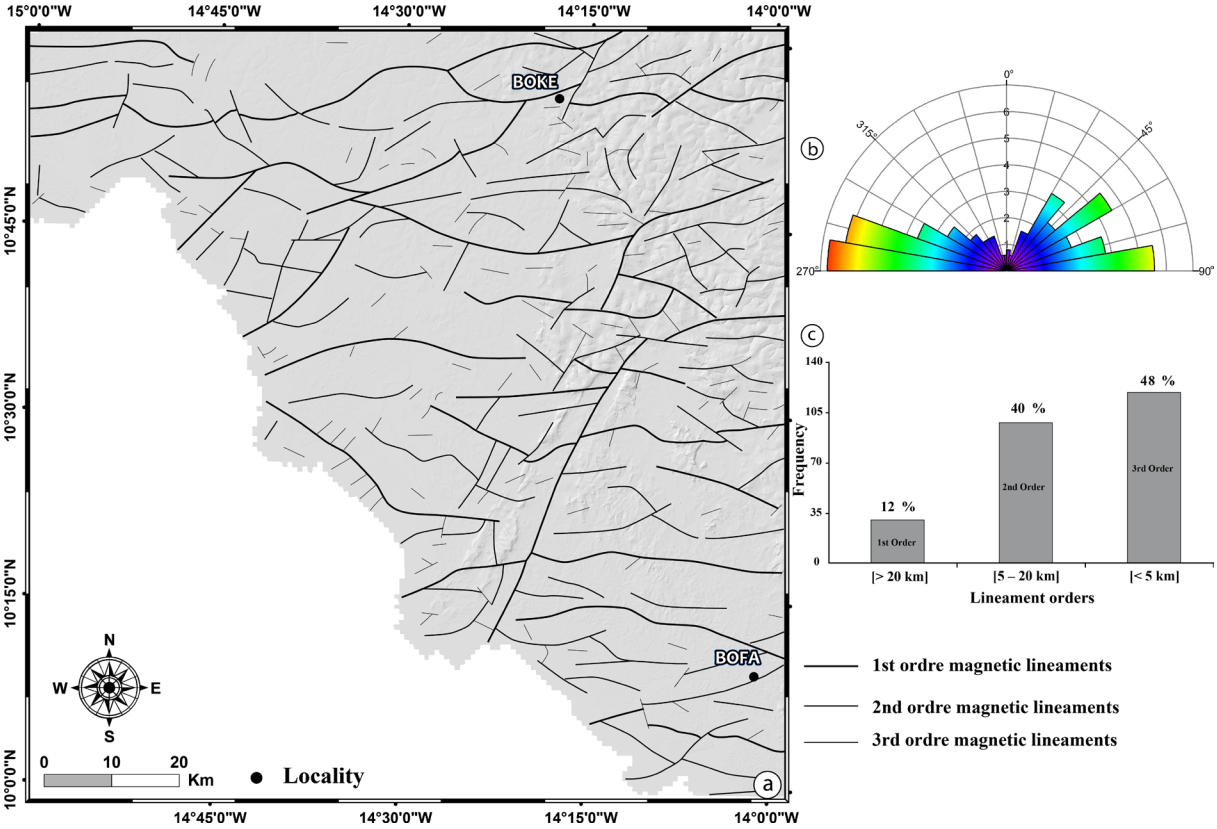


Figure 10. (a) Synthetic structural map of the study area. (b) Rose diagram of lineament orientations. (c) Frequency distribution of the three lineament orders.

the more abundant third-order lineaments (<5 km; 48%) are confined to the shallow crust and disappear rapidly with upward continuation.

The sigmoidal geometry of the deep-seated lineaments is characteristic of ductile shear zones, while the lateral displacement of TAHG maxima between successive continuation levels indicates the coexistence of both steeply dipping and moderately inclined structures at depth. These observations suggest a vertically organized structural architecture reflecting successive tectonic episodes. The deep curvilinear structures are interpreted as inherited ductile shear zones developed during the Eburnean and Pan-African orogenic events, which are regionally expressed by pervasive foliation, mylonitization, and transpressional to thrust-related deformation within the Precambrian basement (Mamedov et al., 2010a; Grenholm et al., 2019). In contrast, the dense network of shallow rectilinear fractures is attributed to later brittle faulting associated with Mesozoic Atlantic rifting and the reactivation of pre-existing basement discontinuities (Mamedov et al., 2010a).

The structural framework identified in this study has important implications for bauxite exploration within the Fouta Djallon-Mandingo bauxite province. Although lateritic bauxite is a near-surface weathering product and is not directly related to the deep magnetic sources, the mapped fault and fracture network, particularly the intersections of the NE-ENE and NW-SE lineament systems, exerts a primary control on drainage, weathering, and laterite development, thereby influencing the distribution of bauxite mineralization (Mamedov et al., 2010a). These results provide a coherent regional model of the basement structural framework as resolved by the available aeromagnetic dataset. Accordingly, the mapped lineament network and depth distributions are interpreted in terms of first-order structural patterns, whereas smaller-scale structural features remain beyond the resolving capability of the dataset. Similarly, the Euler depth estimates are considered to represent broad structural levels and the relative distribution of magnetic source depths rather than unique geometrical solutions. As the present interpretation is derived from legacy aeromagnetic data, future integration with complementary geological and geophysical information, including field structural observations, gravity data, satellite-derived lineaments, rock magnetic measurements, and geochronological constraints, would further refine the proposed structural framework and its tectonic interpretation.

6. Conclusion

This study used high-resolution aeromagnetic data to characterize the concealed structure of the Boke region in north-western Guinea, where a thick Paleozoic sedimentary cover and a lateritic mantle hide the basement of the West African Craton margin. An integrated workflow combining reduction to the equator, upward continuation at four levels (2, 4, 6 and 8 km), the analytic signal, the horizontal gradient amplitude, the tilt derivative, the tilt angle of the horizontal gradient (TAHG) at each continuation level, and Euler deconvolution was applied to map the structural framework and to estimate the depth of the magnetic sources. Three magnetic domains were identified. Two positive anomalies, PMA1 and PMA2, are attributed to concealed mafic bodies, shallow Mesozoic dolerite sills and dykes for PMA2, and deep Birimian metagabbroic or Archean mafic basement for PMA1 and are separated by a broad negative anomaly (NMA1) produced by the weakly magnetic sedimentary fill of the Bowe Basin. Euler deconvolution gave source depths between about 400 m and 9,600 m. The deepest solutions forming an arcuate band beneath the northern part of the area and the shallowest contacts bounding and dissecting the central basin. The magnetic lineaments, classified into three orders by length, define a polyphase fault network. The most frequent set trends WNW-ESE to E-W and reflects an inherited sublatitudinal basement fabric, whereas the NE-SW to ENE-WSW set, although less frequent, is the principal tectonic direction and corresponds to the Mesozoic transform system related to the opening of the Atlantic Ocean. The multi-level analysis also revealed a clear depth-stratified architecture, in which a dense, shallow, brittle fracture fabric passes downward into a few long, curvilinear and sigmoidal deep structures indicative of ductile shear. This organization is interpreted as an inherited Eburnean-Pan-African transcurrent framework overprinted by later Mesozoic brittle faulting. These results clarify the tectonic architecture of this segment of the West African Craton margin and are also of practical interest. By mapping the fault and fracture framework, and especially the structural intersections that control weathering, drainage and plateau preservation, the study provides a structural guide to the development and preservation of the lateritic bauxite for which the region is known. The workflow and in particular the multi-level TAHG shows the value of aeromagnetic data for depth-resolved structural analysis and offers a transferable approach for basement characterization in other cover-masked cratonic areas. Field structural mapping, gravity data and geochronology will nonetheless be needed to validate and refine the interpretations proposed here.

Data availability statement. The aeromagnetic data used in this study were acquired during airborne surveys conducted in 1980-1981 under the authority of the Guinean Ministry of Mines and Geology. The raw survey data are owned by the Ministry and are not publicly available, being subject to its data-sharing policies. The derived interpretation products generated during this study including the magnetic lineament data, the Euler deconvolution depth solutions, and the structural interpretation layers are available from the corresponding author upon reasonable request.

References

Akaemov, S. T. (1975). Lithology and Genesis of the Bauxites of Sangaredy(Western Africa), Paper from" Probl. Genezisa Boksitov", Nauka, Moscow. 1975, 235-246, (Russian).

Awoyemi, M. O., O. D. Ajama, O. S. Hammed, A. B. Arogundade and S. C. Falade (2018). Geophysical mapping of buried faults in parts of Bida Basin, North Central Nigeria, Geophys. Prospect., 66, S1, 40-54.

Baranov, V. and H. Naudy (1964). Numerical calculation of the formula of reduction to the magnetic pole, Geophys., 29, 1, 67-79.

Barry, A. D., M. Cissé, M. M. Parfait and M. M. Hallarou (2021). Mineralogical and Geochemical Characteristics of the Sangarédi Bauxite Deposit, Boké Region, Republic of Guinea, Environ. Earth Sci. Res. J., 8, 1.

Benyas, K. et al. (2021) Exploiting aeromagnetic and gravity data interpretation to delineate massif deposits of Rehamna Area (Western Meseta-Morocco), The Iraqi Geological Journal, 52, 2C, 13-28.

Bessoles, B. (1977). Géologie de l'Afrique. Le Craton Ouest Africain. Mémoires du Bureau de Recherches Géologiques et Minières, 88. Orléans: BRGM, 402 p.

Blakely, R. J., R. E., Wells, T. S. Yelin, I. P. Madin and M. H. Beeson (1995). Tectonic setting of the Portland-Vancouver area, Oregon and Washington: Constraints from low-altitude aeromagnetic data, Geol. Soc. Am. Bull, 107, 9, 1051-1062.

Blakely, R. J. and R. W. Simpson (1986). Approximating edges of source bodies from magnetic or gravity anomalies, Geophys., 51, 7, 1494-1498, doi:10.1190/1.1442197.

Boher, M. et al. (1992). Crustal growth in West Africa at 2.1 Ga, J. Geophys. Res.: Solid Earth, 97, B1, 345-369, doi:10.1029/91JB01640.

Bouiflane, M., A. Manar, F. Medina, N. Youbi and A. Rimi (2017). Mapping and characterization from aeromagnetic data of the Foum Zguid dolerite Dyke (Anti-Atlas, Morocco) a member of the Central Atlantic Magmatic Province (CAMP), Tectonophys., 708, 15-27.

Boulangé, B., G. Bouzat and M. Pouliquen (1996). Mineralogical and geochemical characteristics of two bauxitic profiles, Fria, Guinea Republic, Mineralium Deposita, 31, 5, 432-438, doi:10.1007/BF00189190.

Briggs, I. C. (1974). Machine contouring using minimum curvature, Geophys., 39, 1, 39-48, doi:10.1190/1.1440410.

Clark, D. A. (1999). Magnetic petrology of igneous intrusions: implications for exploration and magnetic interpretation, Explor. Geophys., 30, 2, 5-26.

Cordell, L. and V. J. S. Grauch (1985). Mapping basement magnetization zones from aeromagnetic data in the San Juan Basin, New Mexico.

Ferreira, F. J., J. de Souza, A. de B. e S. Bongiolo and L. G. de Castro (2013). Enhancement of the total horizontal gradient of magnetic anomalies using the tilt angle, Geophys., 78, 3, J33-J41.

Grant, F. S. (1972). Review of data processing and interpretation methods in gravity and magnetics, 1964-71, Geophys., 37, 4, 647-661.

Grauch, V. J. S. and L. Cordell (1987). Limitations of determining density or magnetic boundaries from the horizontal gradient of gravity or pseudogravity data, Geophys., 52, 1, 118-121.

Grenholm, M., M. Jessell and N. Thébaud (2019). A geodynamic model for the Paleoproterozoic (ca. 2.27-1.96 Ga) Birimian Orogen of the southern West African Craton-Insights into an evolving accretionary-collisional orogenic system, Earth-Sci. Rev., 192, 138-193.

Hartman, R. R., J. L. Friedberg and D. J. Teskey (1971). A system for rapid digital aeromagnetic interpretation, Geophysics, 36, 5, 891-918.

Henderson, R. G. and I. Zietz (1949). The upward continuation of anomalies in total magnetic intensity fields, Geophysics, 14, 4, 517-534.

Hinze, W. J., R. Von Frese and A. H. Saad (2013). Gravity and magnetic exploration: Principles, practices, and applications. Cambridge University Press.

Hoppe, R. W. (1977). Sangaredi an African plateau of bauxite. Engineering Mining J., 178, 8, 83-90.

Ibraheem, I. M., M. Haggag and B. Tezkan (2019). Edge detectors as structural imaging tools using aeromagnetic data: a case study of Sohag Area, Egypt, Geosciences, 9, 5, 211.

Jacobsen, B. H. (1987). A case for upward continuation as a standard separation filter for potential-field maps, Geophys., 52, 8, 1138-1148. doi:10.1190/1.1442378.

Jayeoba, A. and D. Odumade (2015). Geological and structural interpretation of Ado-Ekiti Southwest and its adjoining areas using aeromagnetic data In: Adapted from extended abstract prepared in conjunction with the oral presentation given at Pacific Section AAPG, SEG and SEPM Joint Technical Conference, Oxnard, California.

Makarova, M. A., V. I. Mamedov, Y. V. Alekhin and E. S. Shipilova (2019, November). The unique role of pore water in lateritic bauxite formation, Republic of Guinea, In Doklady Earth Sciences, 489, 1,1297-1300, Moscow: Pleiades Publishing.

Mamedov, V. I. et al. (2021). The World's Largest Fouta Djallon-Mandingo Bauxite Province (West Africa): Part 2. The Effect of Parent Rock Composition on the Abundance and Quality of Bauxites, Geology of Ore Deposits, 63, 6, 599-624, doi:10.1134/S1075701521050044.

Mamedov, V. I., Y. V. Boufeev and Y. A. Nikitine (2010a). Geology of the Republic of Guinea', Ministry of Mines and Geology of the Republic of Guinea, Geoprospects LTD [Preprint].

Mamedov, V. I., Y. V. Boufeev and Y. A. Nikitine (2010b). Carte gîtologique de la Guinée a 1/50 0 000. Minist. Mines Géologie Géoprospect Ltd Univ. D'États E Moscou M Lomonossov Conakry-Moscou., Moscou: Aquarel [Preprint].

Mamouch, Y. et al. (2023). Aeromagnetic data of the Kelâat M'Gouna inlier (Jbel Saghro, Eastern Anti-Atlas, Morocco): Geotectonic and mining implications, J. African Earth Sci., 197, 104744.

Marson, I. and E. E. Klingele (1993). Advantages of using the vertical gradient of gravity for 3-D interpretation.,Geophys., 58, 11, 1588-1595.

Miftah, A., D. El Azzab, A. Attou and A. Manar (2017). Contribution of the geomagnetism to the region of the massif Jbel Saghro geology, Eastern Anti-Atlas, Morocco, Arabian J. Geosci., 10, 21, 460.

Miller, H. G. and V. Singh (1994). Potential field tilt – a new concept for location of potential field sources', J. Appl. Geophys., 32, 2-3, 213-217.

Minty, B. R. S. (1991). Simple micro-levelling for aeromagnetic data, Explor. Geophys., 22, 4, 591-592.

Mohamed, A., M. Abdelrady, F. Alshehri, M. A. Mohammed and A. Abdelrady (2022). Detection of mineralization zones using aeromagnetic data, Appl. Sci., 12, 18, 9078.

Nabighian, M. N. et al. (2005). 75th Anniversary-The historical development of the magnetic method in exploration', Geophys., 70, 6, 33ND-61ND.

Nabighian, M. N. (1972). The analytic signal of two-dimensional magnetic bodies with polygonal cross-section: its properties and use for automated anomaly interpretation, Geophys., 37, 3, 507-517.

Ouchchen, M. et al. (2021). Structural interpretation of the Igherm region (Western Anti Atlas, Morocco) from an aeromagnetic analysis: Implications for copper exploration, J. African Earth Sci., 176, 104140, doi:10.1016/j.jafrearsci.2021.104140.

Phillips, J. D. (2007). Geosoft eXecutables (GX's) developed by the US Geological Survey, version 2.0, with notes on GX development from Fortran code, 111, US Geological Survey.

Reeves, C. (2005). Aeromagnetic surveys: principles, practice and interpretation, 155, 30, Washington (DC): Geosoft.

Reid, A. B. et al. (1990) Magnetic interpretation in three dimensions using Euler deconvolution, Geophys., 55, 1, 80-91, doi:10.1190/1.1442774.

Reid, A. B., J. Ebbing and S. J. Webb (2012). Comment on: A crustal thickness map of Africa derived from a global gravity field model using Euler deconvolution by G. E. Tedla, M. van der Meijde, A. A. Nyblade and F. D. van der Meer, Geophys. J. Int., 189, 3, 1217-1222.

Roest, W. R., J. Verhoef and M. Pilkington (1992). Magnetic interpretation using the 3-D analytic signal, Geophys., 57, 1, 116-125.

Salem, A. et al. (2007). Tilt-depth method: A simple depth estimation method using first-order magnetic derivatives, The Leading Edge, 26, 12, 1502-1505, doi:10.1190/1.2821934.

Salem, A. et al. (2008). Interpretation of magnetic data using tilt-angle derivatives, Geophys., 73, 1, L1-L10, doi:10.1190/1.2799992.

Sangaré, A. et al. (2024). Mapping bauxite-associated alterations in the Boke region (NW part of Republic of Guinea), using the airborne gamma-ray spectrometry data, Scientific African, 24, e02184, doi:10.1016/j.sciaf.2024.e02184.

Shehu, A. T., L. I. Nwankwo and K. A. Salako (2017). The Source Parameter Imaging (SPI) method for estimation of depth to buried magnetic sources from gridded digital data of the Sokoto Basin, Nigeria: Implications in Exploration Geophysics, Zimbabwe Journal of Science and Technology, 12, 1, 66-72.

Sidibe, M. and M. G. Yalcin (2019). Petrography, mineralogy, geochemistry and genesis of the Balaya bauxite deposits in Kindia region, Maritime Guinea, West Africa, Jo. African Earth Sci., 149, 348-366.

Smith, W. H. and P. Wessel (1990). Gridding with continuous curvature splines in tension, Geophys., 55, 3, 293-305, doi:10.1190/1.1442837.

Swain, C. J. (1976). A FORTRAN IV program for interpolating irregularly spaced data using the difference equations for minimum curvature, Compu. Geosci., 1, 4, 231-240.

Telford, W. M., L. P. Geldart and R. E. Sheriff (1990). Applied geophysics (2nd ed.). Cambridge: Cambridge University Press. xx + 770 pp.

Thompson, D. T. (1982). EULDPH: A new technique for making computer-assisted depth estimates from magnetic data, Geophys., 47, 1, 31-43.

Verduzco, B. et al. (2004). New insights into magnetic derivatives for structural mapping, The Leading Edge, 23, 2, 116-119, doi:10.1190/1.1651454.

Wright, J. B., D. A. Hastings, W. B Jones and H. R.Williams (1985). Geology and mineral resources of West Africa, 187, London: Allen & Unwin.

Zhu, X., L. Wang and X. Zhou (2022). Structural features of the Jiangshao Fault Zone inferred from aeromagnetic data for South China and the East China Sea, Tectonophysics, 826, 229252.

***CORRESPONDING AUTHOR: Lahsen ACHKOUCH**,
Hassan First University of Settat, Faculty of Sciences and Technology, Laboratory Physico Chemistry of Processes and Materials, Research Team Geology of the Mining and Energetics Resources, Settat 26002, Morocco.
e-mail: l.achkouch@uhp.ac.ma

© 2026 the Author(s).
Open Access. This article is licensed under a Creative Commons Attribution 4.0 International License